Structural Engineering and Mechanics, *Vol. 61, No. 5 (2017) 625-635*
DOI: https://doi.org/10.12989/sem.2017.61.5.625

Behavior modeling and damage quantification of confined concrete under cyclic loading

Kabir Sadeghi* and Fatemeh Nouban[a]

Civil Engineering Department, Near East University, Near East Boulevard, ZIP: 99138, Nicosia, North Cyprus, via Mersin 10, Turkey

(Received July 11, 2016, Revised October 26, 2016, Accepted October 28, 2016)

Abstract. Sets of nonlinear formulations together with an energy-based damage index (DI) are proposed to model the behavior and quantify the damage of the confined and unconfined concretes under monotonic and cyclic loading. The proposed formulations and DI can be employed in numerical simulations to determine the stresses and the damages to the fibers or the layers within the sections of reinforced concrete (RC) components. To verify the proposed formulations, an adaptive finite element computer program was generated to simulate the RC structures subjected to monotonic and cyclic loading. By comparing the simulated and the experimental test results, on both the full-scale structural members and concrete cylindrical samples, the proposed uniaxial behavior modeling formulations for confined and unconfined concretes under monotonic and cyclic loading, based on an iterative process, were accordingly adjusted, and then validated. The proposed formulations have strong mathematical structures and can readily be adapted to achieve a higher degree of precision by improving the relevant coefficients based on more precise tests. To apply the proposed DI, the stress-strain data of concrete elements is required. It can easily be calculated by using the proposed nonlinear constitutive laws for confined and unconfined concretes in this paper.

Keywords: confined/unconfined concrete; monotonic/cyclic loading; damage quantification; numerical modeling

1. Introduction

In the literature, many models can be found to determine the behavior model and damage of confined and unconfined concretes. Each model has its own limitation, application condition, advantage and disadvantage. Since the aim of some models is the determination of the ultimate strength of RC elements, the models covering both the confined and unconfined concretes under continuous monotonic and cyclic loading, serving as input for continuous behavior modeling and damage quantification of RC elements, are attractive.

Over the past years, many researchers, such as Soh and Bhalla (2005), Amziane and Dubé (2008), Malecot *et al.* (2010), Yu *et al.* (2010), Poinard *et al.* (2010), Markovich *et al.* (2011), Chen *et al.* (2011) and Cao and Ronagh (2013) have proposed different formulations for damage index (DI) for concrete.

Stress, strain, stiffness and modulus are the main parameters employed in these damage indices.

Yu *et al.* (2010) proposed a DI for concrete subjected to uniaxial compression that is defined as one minus the ratio of decaying stress on the descending branch to the peak stress. With the same pattern, Soh and Bhalla (2005) defined a DI for concrete in term of stiffness instead of stress. They defined DI as one minus the ratio of damaged stiffness to the initial stiffness. Chen *et al.* (2011) defined a DI for concrete as the ratio of losing modulus to the initial modulus. They defined DI as one minus the ratio of damaged modulus to the initial modulus. Amziane and Dubé (2008) defined a DI for concrete, using the modulus of concrete. They defined DI as one minus the ratio of the initial reloading modulus of concrete at any stage of reloading to the secant Young modulus defined at the stress of 40% of the ultimate strength of concrete. Cao and Ronagh (2013) investigated the damage of concrete subjected to monotonic compressive loading using four different damage models and proposed a simple model to evaluate the damage of concrete.

The concrete damage model that is implemented in the LS-DYNA code (2007) is capable to simulate the behavior of unconfined concretes subjected to complex static and dynamic loads.

Nevertheless, the values for the numerous parameters, that are required as an input, are not provided by the code. Markovich *et al.* (2011) have calibrated the LS-DYNA code damage model for a wide range of concretes, using triaxial-compression-test data obtained from the literature. Although, not enough validation has been carried out in the tests, but their calibrated model demonstrates better agreement with published test results than the model available in LS-DYNA.

An energy based DI for confined and unconfined concretes is proposed in this paper. To determine the proposed DI, the stress-strain data for concrete elements is required.

Several models have been proposed to determine the behavior law of compressive unconfined concrete and concrete confined within rectangular or spiral stirrup ties. The significant lateral passive compression and strain on

*Corresponding author, Professor
E-mail: kabir.sadeghi@neu.edu.tr
[a]Assistant Professor

Copyright © 2017 Techno-Press, Ltd.

ISSN: 1225-4568 (Print), 1598-6217 (Online)

concrete due to the confinement generated by the transverse reinforcements, indicates that the concrete is in the state of tri-axial compression. In this condition, the concrete element is very ductile.

Researchers such as Mander *et al.* (1984), Park *et al.* (1982) performed several tests on real full-scale structures.

The primary researches on the behavior law of confined concrete were performed generally on a small scale on samples under the concentrated point loading by applying a quasi-static strain velocity.

Meyer (1988), CEB (1988) and others proposed equations for the stress-strain model of concrete confined by spiral or circular transverse reinforcements. Chore and Shelke (2013) proposed a method to establish a predictive relationship between properties and proportions of ingredients of concrete, compaction factor, weight of concrete cubes and strength of concrete whereby the strength of concrete can be predicted at an early age.

Markovic *et al*. (2006) have introduced a coupled elasto-plastic and damage constitutive model with the stress field as the independent variable. The damage part is described in an analogous way to the classical plasticity models, which enables an efficient use of the complementary variational formulation. They worked out the complete numerical implementation and showed its efficiency with respect to the more classical displacement based formulation. They demonstrated the particular advantage of using their proposed approach within the framework of structured representation of a heterogeneous material. They showed the advantages of the stress based finite element formulation when applied to nonlinear inelastic material behavior like plasticity or damage.

In the following, a model for confined and unconfined concretes under monotonic and cyclic compression loading is proposed.

The goal of this paper is to present nonlinear stress-strain laws along with an energy-based DI for confined and unconfined concretes, applied to simulate the concrete finite elements within the sections of RC components subjected to monotonic and cyclic loading.

2. Experimental data and reference column

The results of the experimental test, performed on the full-scale columns by Garcia Gonzalez (Garcia Gonzalez 1990, Sieffert *et al.* 1990), Park and Kent (1972) are mainly used for the global validation of the proposed models. Over 20 tests were performed at the University of Nantes on columns under biaxial alternating cyclic with axial loading. The dimensions and characteristics of the columns tested by Garcia Gonzalez are as follows: rectangular section 18 cm×25 cm, height of 1.75 m, four longitudinal reinforcements with a diameter of 12 mm (ϕ12), concrete of strength of 42 MPa, stirrup ties of diameter 6 mm with a longitudinal spacing of 9 cm, yielding stress of steel bars: 470 MPa. These columns were fixed at the bottom, free at the top and were under an axial force of 500 kN and the cyclic oriented lateral force and axial loading or the oriented pushover force and axial loading in any direction at the top. In this paper, Garcia Gonzalez's Column is called "reference column" and its section is called "reference section".

The experimental test results on the confined and unconfined concrete samples performed by Sadeghi (2002), Al Sulayfani (1986), CEB (1988), Park and Kent (1972), Buyukozturk (1985), Meyer (1988), Karsan and Jirsa (1964), Mander *et al.* (1984) are also used for local validation. Over 55 cylindrical samples of confined and unconfined concretes were also tested by Sadeghi (2002).

Since unconfined concrete under cyclic loading and also confined concrete under monotonic loading are special cases of confined concrete under cyclic loading, the models of Al Sulayfani (1988) (for unconfined concrete under cyclic loading case) and CEB (1988) (for confined concrete under monotonic loading case) are modified and used for validation of particular cases of the proposed models.

The simulated results obtained by using the proposed models are also compared with the results reported in literature.

3. Developed finite element computer program

A computer program entitled Column Analysis and Damage Evaluation Program (CADEP) has been developed by Sadeghi (2015) to simulate numerically the behavior of RC columns under cyclic loading and DI for rectangular or nonrectangular sections, considering the nonlinear behavior of materials.

CADEP has some sub-programs such as BBCS (biaxial bending column simulation) which is used as Base Model, CCS (confined concrete simulation), UCS (unconfined concrete simulation), SBS (steel bars simulation), EC (energy calculation) and DIC (damage index calculation).

In the CADEP computer program, the column is decomposed into two Macro-Elements (MEs) positioned between the inflection point (zero moment) and the critical sections (maxim moments). Then the nonlinear behavior of MEs are analyzed. In fact, a Macro-Element acts as fixed bottom-free top half-column under biaxial cyclic bending moment (i.e., lateral force in any direction) with axial load. Finally, the two connected MEs are assembled to determine the global behavior of the column. To find the status of the entire column, the applied loads and also the secondary moments, due to P-Δ effect, are considered in the simulation of the column. Each section of the column is discretized into fixed rectangular finite elements. For each concrete and reinforcement element a uniaxial behavior is considered and their strain distributions are assumed to form a plane, which remains a plane during deformation (Kinematics Navier's hypothesis). The stresses of concrete and steel are expressed as nonlinear functions of strains in each concrete and steel element. For compressive confined and unconfined concrete elements, the monotonic and cyclic stress-strain models proposed by the authors in this paper and for reinforcements, the expression proposed by Park and Kent (1972) based on the Ramberg-Osgood monotonic and cyclic models have been used in the CADEP. The concrete tensile stress is assumed to be linear

up to the concrete tensile strength. It is assumed that there is a prefect bonding between concrete and steel bars. The CEB-FIP Code (1993) specification is used for the maximum compressive strain value for unconfined concrete. This is particularly applicable where there is a loss of concrete cover outside the stirrups. To determine the failure of confined concrete in the simulation, the equation proposed by Sheikh (1982) has been used.

The basic equilibrium is justified over a critical hypothetical cross-section assuming the Navier law with an average curvature. The method used qualifies as a "strain plane control process" that requires the resolution of a quasi-static simultaneous equation system using a triple iteration process over the strains (Sadeghi 2015). The calculations are based on the monotonic and cyclic nonlinear stress-strain relationships for concrete and reinforcement FE. In order to reach equilibrium, three main strain parameters; the strains at the extreme compressive point, the strains at the extreme tensile point and the strain at a point located at another corner of the section are used as three main variables. For non-rectangular sections these points may be outside the actual cross-sections and be located on the discretizing mesh frontiers.

The nonlinear responses of a Macro-Element and the column are based mainly on the fixed finite elements on the critical sections and on the location of the inflection point. For the entire column, deflection is evaluated using an elastic-plastic analytic formulation (Priestley and Park 1987). The program takes into account the confining effect of the transverse reinforcement and simulates the loss of the concrete cover. The CADEP allows the determination of the failure, the internal local behavior of critical sections (i.e. strains, stresses, neutral axis position, crack positions, loss of material, microscopic DI, etc.) and the external global behavior of the column (curvature, deflection, stiffness, damping ratio, different types of energies for negative and positive displacements, global and local damage indices proposed by Sadeghi and Nouban (2016), etc.).

The simulated results obtained using CADEP are in the main confirmed by the full-scale experimental results obtained by other researchers (Garcia Gonzalez 1990, Sieffert 1990, Park and Kent 1972).

In the CADEP program, a behavior law for confined and unconfined concretes is considered and the behavior laws of the columns are specified. After an iterative process the simulated and experimental results are compared, and then, the confined and unconfined concrete laws are adjusted accordingly. The selected laws, presented here are simple but sufficiently accurate to be used in the monotonic and cyclic numerical simulations.

4. Proposed stress-strain law for confined and unconfined concretes

4.1 Verification methodology

In order to eliminate the problem of scale effect, in addition to using the results of experimental tests on concrete samples, by applying the CADEP computer program, the simulated and experimental test results on the full-scale columns were compared. In this way the proposed nonlinear stress-strain models for confined and unconfined concretes under monotonic and cyclic loading was modified and validated.

The stress-strain curve of unconfined concrete under monotonic loading is used as the envelope curve for the cyclic loading case as confirmed by the Sadeghi (1995, 2002), Karsan and Jirsa (1969), Al Sulayfani (1986). A similar relationship also holds for confined concrete (Mander *et al*. 1984). This, confirmed the relationship between the monotonic and cyclic loading curves used in the proposed models.

4.2 Examples of evaluation and modification of the parameters

Utilization of an unconfined model similar to that of Al Sulayfani (1986) for the simulation of RC element's behavior results in more closely spaced hysteresis loops than are obtained by the experimental tests on the columns of Garcia Gonzalez (1990). To further investigate the problem, the models of Park and Kent (1972), Buyukozturk (1985), Meyer (1988), Karsan and Jirsa (1969) were studied.

Comparative studies on the parameters relating to the point of unloading (slope at the point of unloading and the coordinates of plastic residual stress) were performed. By performing numerical simulation on the reference columns using CADEP and comparing these results with the experimental test of Garcia Gonzalez (1990), it was observed that, the values of unloading tangent modulus E_{U0} and plastic residual strain ε_r (the plastic residual strain is defined as the residual axial strain of concrete when it is unloaded to zero stress (Abbasnia and Holakoo 2012) (see Fig. 3)), which are used for generating the stress-strain $(\sigma - \varepsilon)$ curve, play a very significant role in the form of the moment-curvature response of the section of an RC member in the unloading phase. As shown in Fig. 3, the variation of E_U is less important, because its effect is situated in the zone of lesser stresses. The plastic residual strain ε_r has a non-negligible role in the failure phenomenon in the case of cyclic loading. If this strain is considered greater than the actual case, the failure appears sooner in the response curve. Conversely, if a value of ε_r smaller than the actual one is adapted, the number of cycles at failure and the values of the displacement and the curvature will reduce. In Table 1,

Table 1 Values of $\varepsilon_r/\varepsilon_0$ obtained by using different models

$\varepsilon_A/\varepsilon_0$	0.3	0.5	0.7	1.0	1.2	1.5	1.7	2.0
Model of Al Sulayfani	0.019	0042	0.081	0.182	0.289	0.528	0.751	1.199
Model of Meyer	0.024	0.068	0.132	0.340	0.442	0.615	0.744	0.960
Model of Karsan	0.052	.101	0.162	0.275	0.365	0.521	0.640	0.840
Model of Buyukozturk	0.079	0.165	0.277	0.496	0.675	0.995	1.240	1.660

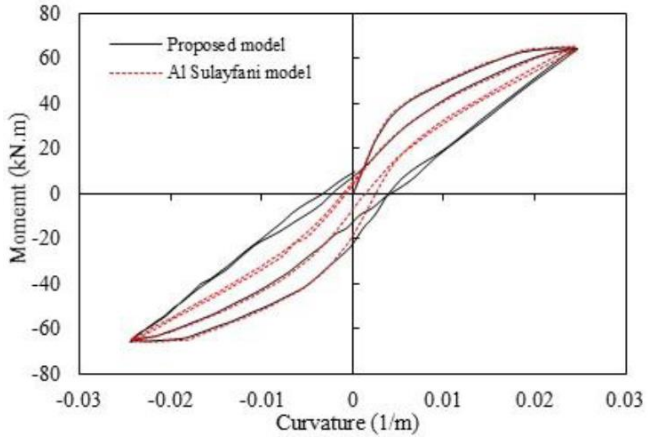

Fig. 1 Moment-curvature response of a rectangular section column for two pairs of E_{U0} and ε_r

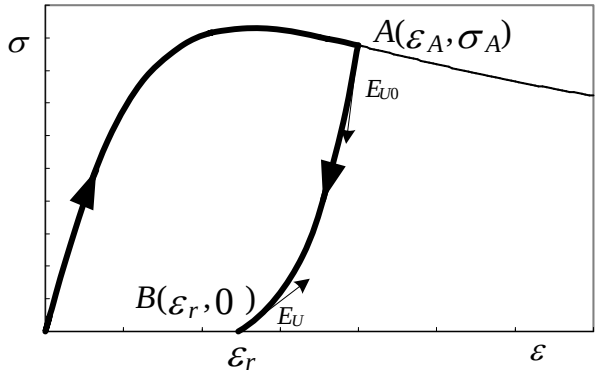

Fig. 3 Unloading from the envelope curve

the variations of the values of $\varepsilon_r/\varepsilon_0$ as a function of $\varepsilon_A/\varepsilon_0$, obtained by using the models proposed by different researchers, are presented (for the definitions of the parameters see Figs. 2 and 3).

Based on the values given in this table, it can be observed that the smaller values of $\varepsilon_r/\varepsilon_0$ are obtained by using Al Sulayfani's model (for $\varepsilon_A/\varepsilon_0$ <1.49) and the biggest values are related to the Buyukozturk model. Comparison of the simulated results using CADEP and the experimental of Meyer, indicates a close agreement between the proposed $\varepsilon_r/\varepsilon_0$ values and the experimental of Meyer values.

As another example, if the value of E_{U0} is assumed to be smaller than the actual case, the hysteresis loops in the response curve (moment-curvature or force-displacement curves) are more closed as shown in Fig. 1. This figure illustrates the moment-curvature response of the reference RC rectangular section of the reference column for two pairs of E_{U0} and ε_r. As shown in this figure, in the loading case (in the first and second positive and negative half cycles), the two curves are very close to each other. Conversely, in the unloading phase, it can be observed that the effects of E_{U0} and ε_r result in a different trajectory for the unloading curve.

These calculations and verifications are performed by applying CADEP program. This kind of verification and comparison with the experimental test results is used to

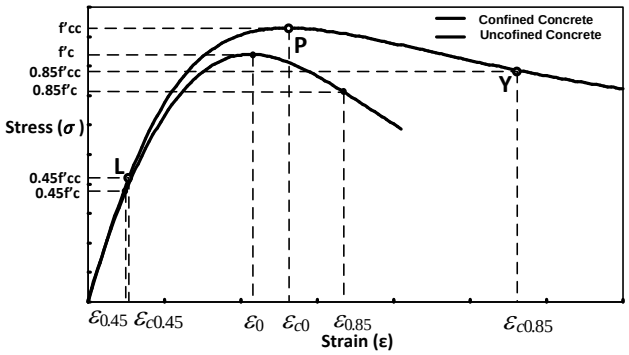

Fig. 2 Parameters employed in the proposed stress-strain curves, monotonic loading cases (Envelope curves for cyclic loading cases)

determine all the parameters and coefficients of the proposed formulations.

4.3 Proposed stress-strain law for confined concrete

The following stress-strain formulations are proposed to simulate numerically the uniaxial behavior of confined and unconfined concrete elements discreted within the sections of RC members.

4.3.1 Stress-strain law for confined concrete under monotonic loading

The proposed analytic equation for the stress-strain law of confined concrete under monotonic compression loading is described below.

Fig. 2 presents schematically the parameters employed in the proposed stress-strain curves for the confined and unconfined concretes under monotonic loading. These curves are also used as the envelope curves in the cyclic loading cases.

The proposed law, presented in Eq. (1), is a simple mathematical model that is valid for confined concretes with the conventional strengths within the range of 20 MPa<f_c'<50 MPa.

$$\sigma = \frac{f_{cc}'}{A_L\,(\frac{\varepsilon}{\varepsilon_{c0}})^2 + B_L\,\left(\frac{\varepsilon}{\varepsilon_{c0}}\right) + C_L + D_L\,(\frac{\varepsilon}{\varepsilon_{c0}})^{-1}} \tag{1}$$

The relationship between the coordinates of the peaks of confined and unconfined concretes (CEB 1988, Sadeghi 1995) are given as:

For $\sigma/f_c' < 0.05$ or $a.\omega_w < 0.1$

$$f_{cc}' = f_c'\,(1.000 + 2.5a.\omega_w) \tag{2}$$

For $\sigma/f_c' \geq 0.05$ or $a.\omega_w \geq 0.1$

$$f_{cc}' = f_c'\,(1.125 + 1.25a.\omega_w) \tag{3}$$

$$\varepsilon_{c0} = \varepsilon_0\left(\frac{f_{cc}'}{f_c'}\right)^2 \tag{4}$$

With

$$\omega_w = k\left(\frac{A_t}{b_{max}\,.\,S_t}\right)(\frac{f_{yt}}{f_c'}) \tag{5}$$

Table 2 Values of k and η for some forms of transverse reinforcements

Form of trans. reinf.									
k*	4	6	6.83	7.22	8	9,33	12.83	10	10.8
η	4	8	8	12	12	12	16	16	16

*k=4 in case of circular transverse reinforcement

$$a = a_n \,.\, a_s \tag{6}$$

$$a_n = 1 - \frac{8}{3\eta} \tag{7}$$

For circular sections, $a_n = 1$.

For rectangular and circular sections

$$a_s = (1 - \frac{S_t}{2\, b_0})^2 \tag{8}$$

For circular sections with spiral transverse reinforcements

$$a_s = (1 - \frac{S_t}{2\, b_0}) \tag{9}$$

Where, σ represents the stress, ε represents the strain, f_c' and f_{cc}' represent compressive strengths of unconfined and confined concretes at 28 days, respectively, ε_0 and ε_{c0} represent the strains related to f_c' and f_{cc}', respectively, A_t represents the cross sectional area of a transverse reinforcement, f_{yt} represents the yield stress of transverse reinforcement, b_{max} represents the larger dimension of the section, S_t represents the longitudinal spacing between transverse reinforcements, a represents the confinement efficiency factor defined as the ratio of the confined area over the total area, a_n represents the transverse reinforcements form factor, a_s represents the transverse reinforcements spacing factor, and b_0 represents the distance between external longitudinal reinforcements in the column section. The factors k and η used in Eqs. (5) and (7) for some forms of transverse reinforcements (CEB 1988, Sadeghi 1995) are given in Table 2.

By inserting the relevant values of stress and strain in Eq. (1) at points *L*, *P* and *Y* and also recognizing that the slope of the curve is equal to zero at the peak of the curve (see Fig. 2), the four unknown coefficients A_L, B_L, C_L and D_L are determined. These four conditions (coordinates of the points *L*, *P* and *Y* and also the slope at point *P*) are determined as follows:

• Point *L* ($\varepsilon_{c0.45}$, $0.45f_{cc}'$) on the confined concrete $\sigma - \varepsilon$ curve:

with

$$\varepsilon_{c0.45} = (0.45\, f_{cc}')/E_{c0.45} \tag{10}$$

and secant modulus

$$E_{c0.45} = 4861\ (f_{cc}')^{0.49} \tag{11}$$

f_{cc}' and $E_{c0.45}$ are expressed in MPa.

• Point *P* at maximum stress of confined concrete $\sigma - \varepsilon$ curve at coordinates (ε_{c0}, f_{cc}')

$$\varepsilon_{c0} = 0.00085\ (f_{cc}')^{0.246} \tag{12}$$

f_{cc}' is expressed in MPa.

$$\sigma_{c0} = f_{cc}' \tag{13}$$

The supplementary condition of zero slope (tangent) at point *P* gives

$$\frac{d\sigma}{d\varepsilon} = 0 \tag{14}$$

• Point *Y* ($\varepsilon_{c0.85}$, $0.85f_{cc}'$) on the confined concrete $\sigma - \varepsilon$ curve:

$$\varepsilon_{c0.85} = \varepsilon_{0.85} + 0.1\omega_w \tag{15}$$

$$\sigma_{c0.85} = 0.85 f_{cc}' \tag{16}$$

where

$$\varepsilon_{0.85} = (1.9 - 0.008 f_{cc}')\varepsilon_0 \tag{17}$$

f_{cc}' is expressed in MPa

4.3.2 Stress-strain law for confined concrete under cyclic loading

Unloading curve

As shown in Figs. 3 to 5, unloading may occur either from the envelope curve or from a phase of reloading. In both cases, Eq. (18) is proposed to give the stress-strain relationship for unloading.

$$\sigma = [A_U \left(\frac{\varepsilon}{\varepsilon_{c0}}\right)^3 + B_U \left(\frac{\varepsilon}{\varepsilon_{c0}}\right)^2 + C_U \left(\frac{\varepsilon}{\varepsilon_{c0}}\right)] f_{cc}' + D_U \tag{18}$$

The four unknown factors A_U, B_U, C_U and D_U can be found by applying the coordinates and slopes of two extreme points on the unloading curve (i.e., the starting and finishing points on the unloading curve).

Case a): Unloading from the envelope curve:

In the case of unloading from the envelope curve (see Fig. 3), to find the unknown factors A_U, B_U, C_U and D_U, the coordinates and slopes at the points $A(\varepsilon_A, \sigma_A)$ and $B(\varepsilon p, 0)$ are employed.

The tangent modulus at point *A* is given as follows

$$E_{U0} = 10\sigma_A/[3(\varepsilon_A - \varepsilon_r)] \tag{19}$$

The plastic residual strain ε_r at point B, depending on the unloading starting point coordinates (point A) can be found from Eq. (20) or (21):

For $\frac{\varepsilon_A}{\varepsilon_{c0}} \leq 1$

$$\varepsilon_r = [0.27 \left(\frac{\varepsilon_A}{\varepsilon_{c0}}\right)^2] \varepsilon_{c0} \tag{20}$$

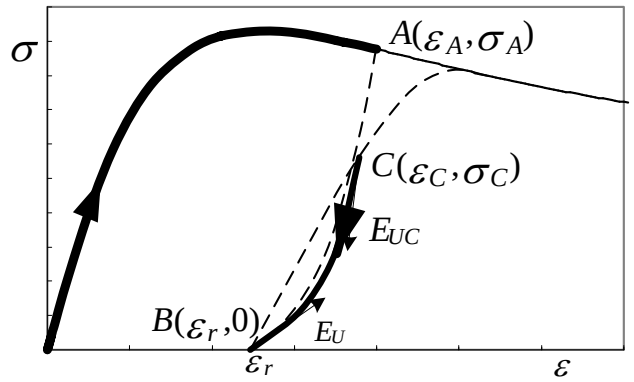

Fig. 4 Unloading from a point *C* on reloading curve when $\varepsilon_C<\varepsilon_A$

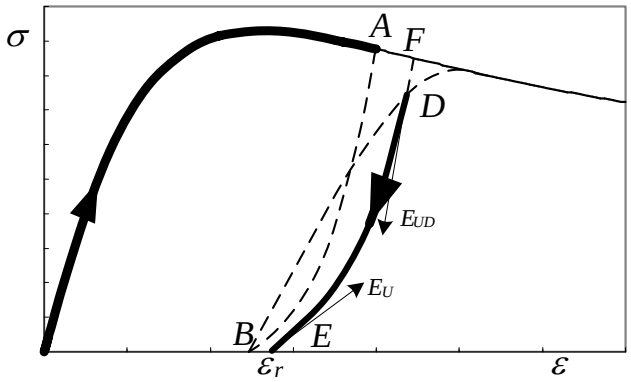

Fig. 5 Unloading from a point *D* on the reloading curve when $\varepsilon_D>\varepsilon_A$

For $\frac{\varepsilon_A}{\varepsilon_{c0}} \geq 1$

$$\varepsilon_r = [0.14\left(\frac{\varepsilon_A}{\varepsilon_{c0}}\right)^2 + 0.2\frac{\varepsilon_A}{\varepsilon_{c0}}]\varepsilon_{c0} \quad (21)$$

The tangent modulus at point B can be found from Eq. (22) or (23):

For $\frac{\varepsilon_r}{\varepsilon_{c0}} < 1$

$$E_U = [\frac{0.72}{0.95 + 6.5\frac{\varepsilon_r}{\varepsilon_{c0}}}]E_{c0.45} \quad (22)$$

For $1.6 \leq \frac{\varepsilon_r}{\varepsilon_{c0}} < 5$

$$E_U = [\frac{\frac{\varepsilon_r}{\varepsilon_{c0}} - 49.99}{48.8}]E_{c0.45} \quad (23)$$

Case b): Unloading from a phase of reloading:

In the case of unloading from a phase of reloading, depending on the coordinates of unloading point (*C* or *D*) comparing with the coordinates of point $A(\varepsilon_A,\ \sigma_A)$, different moduli are used as given below and as shown in Figs. 4 and 5.

b1) Unloading from a point C where $\varepsilon_C < \varepsilon_A$

• Point C($\varepsilon_C,\ \sigma_C$):

The coordinates of point A have been determined in the previous step.

The value of unloading tangent modulus (E_{UC}) at point *C* is obtained by linear interpolation between the modulus E_{U0} at point *A* and E_U at point *B* which is given in Eq. (24)

$$E_{UC} = E_{U0} - \frac{(E_{U0} - E_U)}{(\varepsilon_A - \varepsilon_r)} \quad (24)$$

• Point *B*(ε_r, 0):

The coordinates of point *B* have been determined in the previous step by applying Eq. (20) or (21). The value of the tangent modulus E_U at point B has also been calculated by using Eq. (22) or (23).

b2) Unloading from a point D where $\varepsilon_D > \varepsilon_A$

For the trajectory shown in Fig. 5, the two points *D* and *E* that the curve *DE* passes through them are determined as follows:

• Point D(ε_D, σ_D):

The coordinates of point *D* have been determined in the previous step.

The value of the unloading tangent modulus (E_{UD}) at point *D* is obtained by linear interpolation between the modulus E_{U0} at point *F* and E_U at point *E*. The point *F* is defined as the intersection of the line of slope $1.5E_{c0.45}$ passing from point *D* with the envelope curve. By applying the coordinates of point *F* instead of the coordinates of point *A*, Eq. (19) allows the determination of the unloading modulus at point *F*. E_{UD} can then be found by using Eq. (25):

$$E_{UD} = E_{U0} - \frac{(E_{U0} - E_U)}{(\varepsilon_F - \varepsilon_r)} \quad (25)$$

• Point *E* (ε_r, 0):

The coordinates of point *E* are determined by applying ε_F instead of ε_A in Eq. (20) or (21).

The value of tangent modulus E_U at point *E* is calculated by applying ε_r of point *E* in Eq. (22) or (23).

Reloading curve

Eq. (26) is proposed for the reloading curve:

$$\sigma = [A_R\left(\frac{\varepsilon}{\varepsilon_{c0}}\right)^3 + B_R\left(\frac{\varepsilon}{\varepsilon_{c0}}\right)^2 + C_R\left(\frac{\varepsilon}{\varepsilon_{c0}}\right) + D_R]f'_{cc} \quad (26)$$

The four unknown factors A_R, B_R, C_R and D_R are found by applying the coordinates and slopes of the two extreme points of the reloading curve (i.e., the starting point of reloading phase and the extreme point on the envelope curve).

As shown in Figs. 6 and 7, reloading from zero stress and reloading from an unloading trajectory are considered in two different cases as follows:

Case a): Reloading from a zero stress status (plastic residual strain)

For the trajectory BG shown in Fig. 6, the two points *B* and *G* that the curve BG passes through them are determined as follows

• Point *B* (ε_r, 0):

The coordinates of point *B* have been determined in the

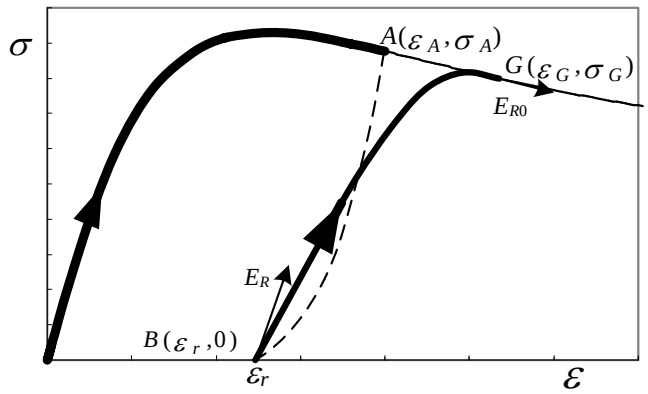

Fig. 6 Reloading from a point of zero stress

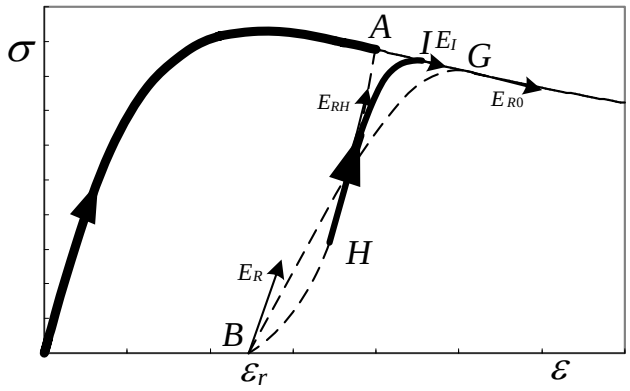

Fig. 7 Reloading from a point on the unloading trajectory

previous steps.

The value of reloading tangent modulus ER at point *B* can be obtained from Eq. (27)

$$E_R = [\frac{1}{0.95 + 2.78\frac{\varepsilon_r}{\varepsilon_{c0}}}]E_{c0.45} \quad (27)$$

• Point *G* (*εG*,*G*)

$$\varepsilon_G = 1.22\varepsilon_A \quad (28)$$

The modulus ER0 is the tangent modulus on the envelope curve at point *G*.

Case b): Reloading from an unloading trajectory

For the trajectory HI shown in Fig. 7, the coordinates and slopes of the two points *H* and *I* at the starting and finishing points of the curve HI are determined as follows:

• Point *H* (*εH*,*H*):

The coordinates of point H have been determined in the previous step.

The tangent modulus ERH at point *H* is considered to be equal to ER and can be calculated by using Eq. (27).

• Point *I* (*εI*,*I*):

The strain at point I is calculated by using Eq. (29)

$$\varepsilon_I = [(K\varepsilon_A - \varepsilon_r) + (1 - K)\varepsilon_H]\frac{\varepsilon_A}{\varepsilon_A - \varepsilon_r} \quad (29)$$

where: $K = 1.22$

The strain at point I, found from Eq. (29), gives $\varepsilon_I = \varepsilon_A$ when $\varepsilon_H = \varepsilon_A$ and gives $\varepsilon_I = \varepsilon_G = K\varepsilon_A$ (see Eq. (28)) when $\varepsilon_H = \varepsilon_r$ (i.e. the point H is positioned on the point *B*).

The stress σ_I and modulus E_I at point *I* can be found by using its strain and the envelope curve.

Failure point:

To determine the maximum compression strain value (ε_{CCU}) of confined concrete, Eq. (30), proposed by Sheikh (1982) was examined and adapted in the formulation

$$\varepsilon_{CCU} = 0.004 + (0.9\rho_s.f_{yh})/300 \quad (30)$$

f_{yh} is expressed in MPa.

where ε_{CCU} presents the maximum compression strain value of confined concrete, ρ_s represents the ratio of transversal reinforcement volume per concrete volume situated inside the stirrups and f_{yh} represents the yielding stress of the stirrups.

4.4 Proposed stress-strain law for unconfined concrete

By replacing the suffixes *cc*, *c*0, *c*0.45, *c*0.85 with *c*, 0, 0.45, 0.85, respectively in Eqs. (1), (10) to (14) and (16) to (29), the proposed stress-strain law for unconfined concrete is found.

To determine the maximum compression strain value (ε_{CU}) of unconfined concrete, Eq. (31) given by CEB-EIP Code (1993) was examined and adapted in the formulation. This equation is particularly applicable where there is a loss of concrete cover outside the stirrups

$$\varepsilon_{CU} = (4 - 0.02f_c')/1000 \quad (31)$$

f_c' is expressed in MPa.

where f_c' represents the conventional 28-days compressive strength of unconfined concrete.

4.5 Application of the proposed formulations

Two examples of the application of the proposed stress-strain laws for confined and unconfined concretes under monotonic and cyclic loading are shown in Figs. 8 and 9.

Fig. 8 shows an example for the application of the proposed model for unconfined concrete and confined concrete with transverse reinforcements (having a 6 cm spacing, and diameters of 8 mm and 6 mm).

It can be seen from Fig. 8 that the presence of the transverse reinforcements significantly increases the strength of the RC elements and this influence is very significant after achieving the ultimate strength (after peak point).

Fig. 9 shows another example of the application of the proposed stress-strain formulation to confined concrete (concrete of 28-days strength of f_c' = 42 MPa, confined within rectangular stirrup ties of diameter 8 mm and a longitudinal spacing of 6 cm) under monotonic and cyclic loading.

4.6 Validation of the proposed stress-strain formulation

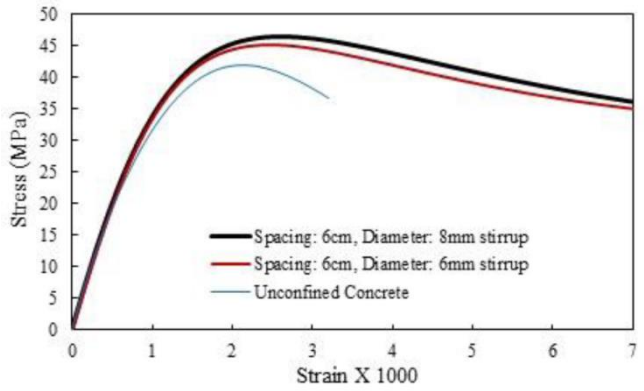

Fig. 8 Effect of the spacing of transverse reinforcements, f_c'=42 MPa

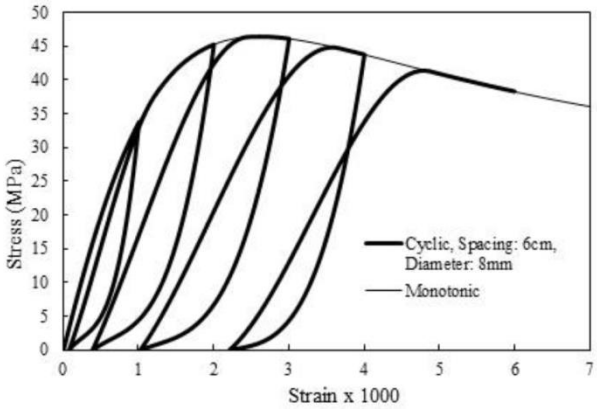

Fig. 9 An example of the application of the proposed stress-strain formulation, f_c'=42 MPa

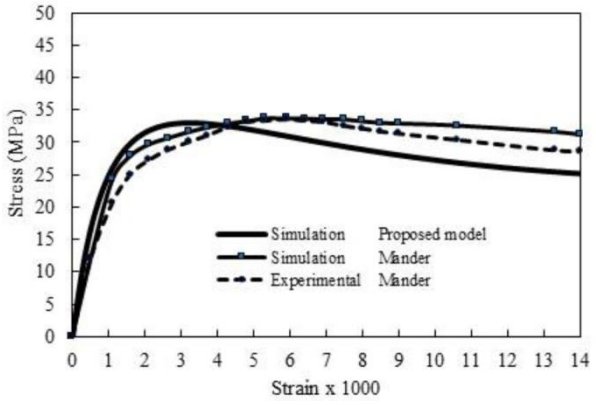

Fig. 10 Comparison of the proposed model with experimental tests and simulation of Mander

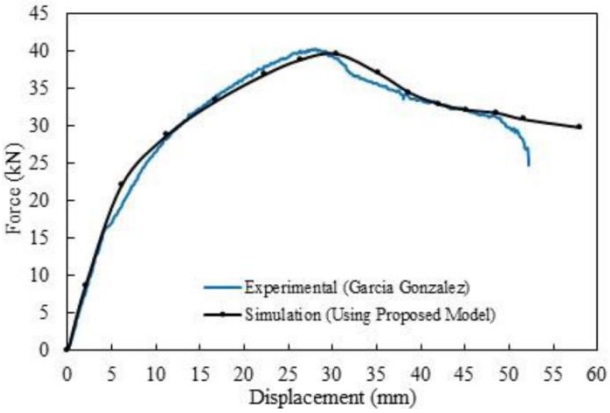

Fig. 11 Comparison of the simulation using the proposed formulation and experimental test, BMAL

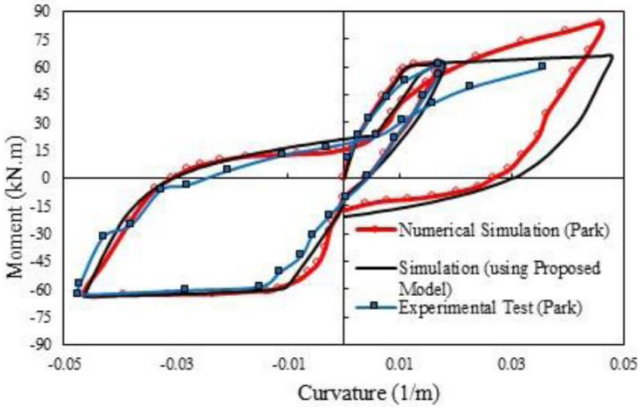

Fig. 12 Comparison of numerical simulation using the proposed model and experimental test/simulation of Park and Kent (1972)

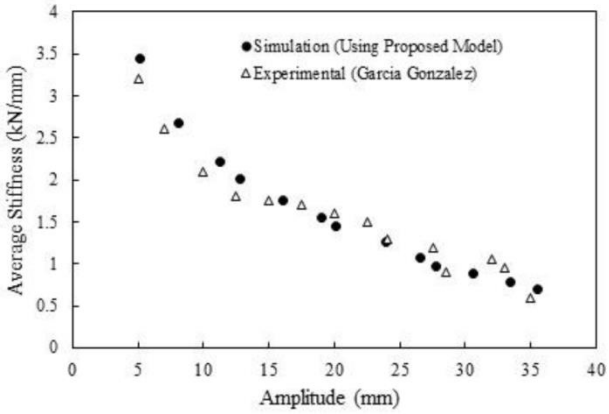

Fig. 13 Comparison of the average stiffness when using the proposed model and experimental tests, cyclic loading, Ω=30°

Some examples of comparison of the simulated results using the proposed stress-strain model and the experimental test results on full-scale RC members are presented in this Section.

The simulated stress values using the proposed formulation for confined concrete, compared with those proposed by Mander (simulation and experimental test results), are illustrated in Fig. 10.

As this figure shows, the location of the peak, i.e., the strain about 6‰ is overestimated by Mander, while this strain and the rate of reduction of stress after the peak in the proposed model fits better with the results of other researchers (e.g.: Belmouden and Lestuzzi (2007) reported the value of the strain at peak of about 0.00267 for the confined concrete with the conventional ultimate strength of f_c'=48 MPa).

The simulated results obtained using CADEP (using the proposed model) were confirmed with the full-scale experimental results obtained by other researchers (Garcia

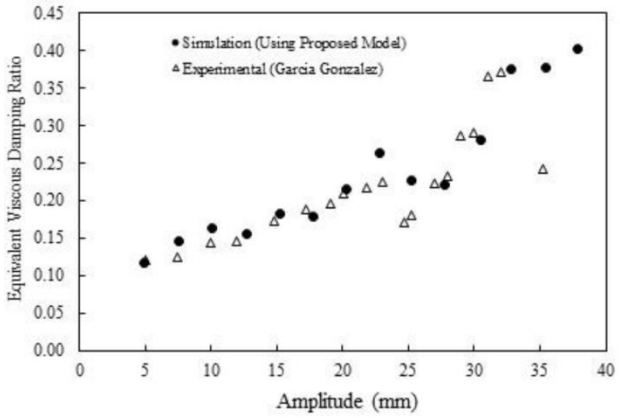

Fig. 14 Comparison of the equivalent viscous damping ratio when using the proposed model and experimental tests, cyclic loading, Ω=30°

Gonzalez 1990, Sieffert *et al*. 1990, Park and Kent 1972).

Comparison of numerically simulated results obtained for RC members using the proposed stress-strain model and experimental tests on the full-scale members are reflected in Figs. 11 to 15. The comparison indicates a good agreement between the proposed simulation and the experimental test results.

In Fig. 11, the simulated results obtained using CADEP (using the proposed model) are compared with the experimental test results of Garcia Gonzalez (1990) on the columns tested under mono-axial bending moment and axial loading (BMAL).

In Fig. 12, the results of the numerical simulation using the proposed model and the experimental test/simulation of Park and Kent (1972) for a cyclic mono-axial bending moment loading case are compared.

As these figures show there is a good agreement between simulated and experimental results.

Figs. 13 and 14 compare the simulated values when applying the proposed model, and the experimental test results (Garcia Gonzalez 1990) for the average stiffness and equivalent viscous damping ratio of the reference columns under cyclic oriented lateral force (the lateral force is applied with the orientation of Ω=30°) and axial loading.

Fig. 15 shows the position of the neutral axis in the critical section of the reference column when the lateral force with the orientation of Ω=45° reaches its maximum value. As shown in this figure, by increasing the lateral force (or moment), the neutral axis moves from outside the section toward the center of the section. When the load is increased, the neutral axis moves with an approximately constant inclination up to the ultimate strength of the section. The results of measurements on the full-scale experimental tests (Garcia Gonzalez 1990), for the neutral axis position when peak load is applied to the critical section of the reference column is shown by the dashed lines in Fig. 15. Experimental test results showed an inclination of α=59° for the neutral axis when peak load was applied on the section for an orientation of lateral force of Ω=45°. As Fig. 15 shows, there is a good agreement between simulated values and experimental results.

In general, comparison of the simulated and

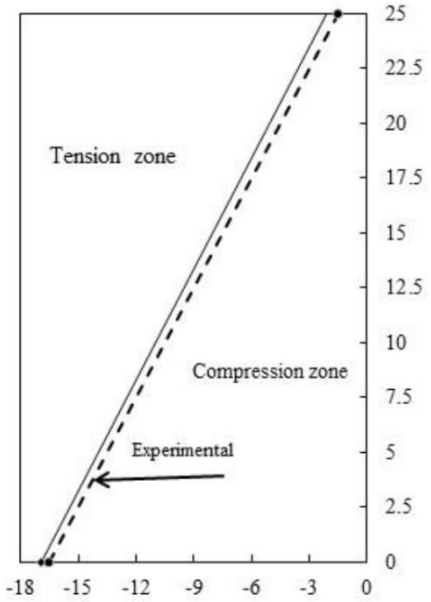

Fig. 15 The neutral axis position of the reference section, maximum load, Ω=45°

experimental test results indicates a close agreement between the simulations using the proposed models and the experimental tests on full-scale RC members.

5. Proposition of a damage index for Concrete

A damage index (DI), applicable to confined and unconfined concrete elements subjected to cyclic and monotonic loading, is proposed as follows.

5.1 "Primary half-cycle" and "following half-cycle" concepts

Following Otes (1985) a "primary half-cycle (PHC)" is considered when any half-cycle reaches a new maximum strain: it is followed by a certain number of "following half-cycles (FHC)" with smaller strains. Whenever a certain maximum strain, corresponding to the primary half-cycle $(PHC)_i$ is exceeded, a new primary half-cycle $(PHC)_{i+1}$ is established. Every PHC corresponds to a certain damage degree.

5.2 Proposed damage index

A damage index (DI) for confined and unconfined concretes under cyclic and monotonic loading is proposed, as given in Eq. (32).

$$DI = \frac{\sum_{i=1}^{i=i} \int_{\varepsilon_{p(i-1)}}^{\varepsilon_{pi}} \sigma_{pi}.d\varepsilon_{pi}}{\sum_{k=1}^{k=n} \int_{\varepsilon_{p(k-1)}}^{\varepsilon_{pk}} \sigma_{pk}.d\varepsilon_{pk}} \quad (32)$$

Where i and k are the cycle numbers, n is the cycle number at concrete failure, σ_{pi} is the applied compressive stress during $(PHC)_i$, $d\varepsilon_{pi}$ is the differential strain during $(PHC)_i$, and $\int_{\varepsilon_{p(i-1)}}^{\varepsilon_{pi}} \sigma_{pi}.d\varepsilon_{pi}$ is the area under the curve of

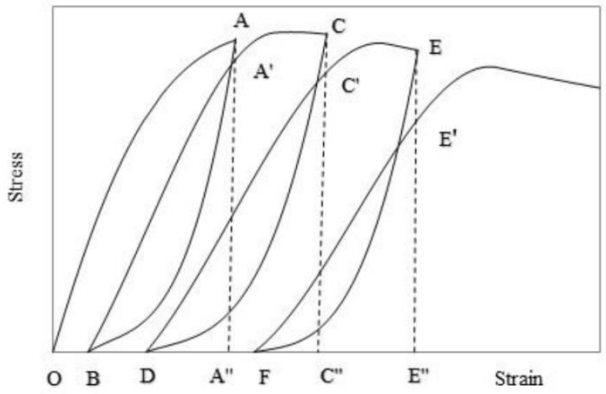

Fig. 16 Schematic illustration of DI calculation procedure for cyclic loading

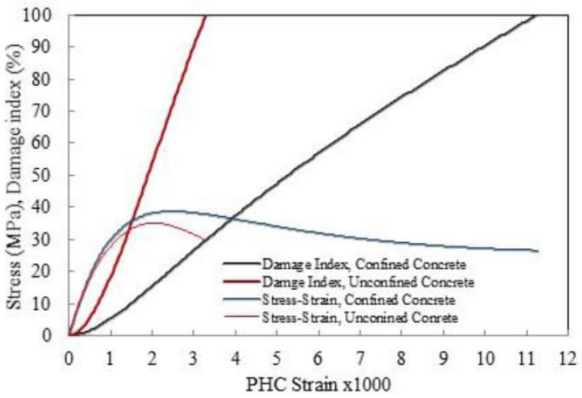

Fig. 17 Proposed DI, calculated for confined and unconfined concretes under cyclic loading

stress-strain during $(PHC)_i$.

The concept and the form of the proposed energy-based DI for concrete is similar to the concept and the form of the global energy-based simplified DI proposed by the authors for the reinforced concrete structures (Sadeghi and Nouban 2016).

To apply the proposed DI for confined and unconfined concretes, the stress-strain data of the concrete element is required.

5.3 Schematic example of applying PHC absorbed energy in DI

The evaluation of the PHC and FHC absorbed energies and DI is illustrated by the following example shown schematically in Fig. 16 for cyclic loading.

Fig. 16 shows typical stress-strain curve of a confined concrete under cyclic loading. The energy E_{p1} of first PHC corresponds to the under curve area of OAA'', whereas E_{f1} of first FHC is still zero. If point A corresponded to failure, E_{p1} would be equal to $\sum_{i=1}^{i=i} E_{pimax}$ and E_u while $i=i_{max}=n=1$ and DI=100%. This concept retains its validity for monotonic loading at failure.

During unloading toward point B, the recovered energy, corresponding to the area under the curve AA''B, is recovered, while the DI retains its value. Further loading up to point A' (maximum strain to date) is equal to the first FHC "following half-cycle", with absorbed energy E_{f1}, corresponding to the under curve area of BA'A''. After point A', a new PHC is formed. E_{p2} is equal to the area under the curve A'CC''A''.

During unloading toward point D, the recovered energy corresponding to the area under the curve CC''D, is recovered, while the DI retains its value.

Further loading up to point C' (maximum strain to date) is equal to the second FHC "following half-cycle", with absorbed energy E_{f2}, corresponding to the under curve area of DC'C''. After point C', a new PHC is formed. E_{p3} is equal to the area under the curve C'EE''C''. Subsequent cycles are analyzed with the same procedure and DI is calculated.

5.4 Different phases of damage and DI

Fig. 17 compares the proposed DI, calculated for: concrete confined within rectangular transverse reinforcements with a diameter of 9 mm and a spacing of 6 cm, along with unconfined concrete of strength of f_c'=35 MPa under cyclic loading.

As Fig. 17 indicates, in this case, the DI is about 55.63% at peak point (34 MPa, 2.05%) of unconfined concrete stress-strain curve and is about 20.92% at peak point (38.62 MPa, 2.50%) of confined concrete stress-strain.

In general, the proposed DI reaches between 50% and 60% at the peak point of the unconfined concrete's stress-strain curve and is between 20% and 25% at the peak point of confined concrete stress-strain curve. It reaches 100% at failure.

It is to be noted that, in monotonic loading case, practically for the strains greater than peak strain, without increasing the load, strain increases up to the failure of concrete, while in cyclic loading case, due to loading, unloading and reloading action, concrete resists for the strains greater than strain at peak. Since the monotonic stress-strain curve acts as envelop of the stress-strain curve in the cyclic loading case, it can be used in DI calculations for cyclic loading case as well.

In order to calculate DI, the stress-strain data for the concrete element is required. This data can be found from the proposed formulations to simulate the concrete behavior. In deciding after an earthquake, whether to repair or demolish a structure, the calculated DI is compared with an allowable damage index ($\overline{DI}$) which could be determined by technical rules and practice building codes for different types of structures according to the economy and safety criteria.

6. Conclusions

The proposed uniaxial stress-strain models for confined and unconfined concretes under the compression monotonic and cyclic loading is simple and applicable to simulate numerically the RC structures' behaviors under monotonic and cyclic loading.

The proposed models are validated mainly by comparison with the results of the experimental tests carried

out on both concrete cylindrical samples and on the RC full-scale columns subjected to cyclic loading performed by different researchers.

Since the proposed formulations have strong mathematical structures, they can readily be adapted to achieve a higher degree of precision by improving the relevant coefficients on more precise tests.

The damage index proposed in this paper is applicable to confined and unconfined concrete elements subjected to cyclic and monotonic loading. It is a practical means for determining whether to repair or demolish structures after an earthquake. It can also be employed in the design of new structures as a design parameter to define the acceptable limit of damage as set by building codes.

Acknowledgements

The financial and technical supports of the Near East University, the University of Nantes (Ecole Central de Nantes)/France and Water Resources Management Organization/Ministry of Energy/Iran are appreciated.

References

Abbasnia, R. and Holakoo, A. (2012), "An investigation of stress-strain behavior of FRP-confined concrete under cyclic compressive loading", *Int. J. Civil Eng.*, **10**(3), 201-209.

Al Sulayfani, B. (1986), "Contribution á l'étude du comportement des ossatures en béton armé sous sollicitations cycliques par analyse non-linéaire globale", Ph.D. Dissertation, University of Nantes/Ecole Central de Nantes, Nantes.

Amziane, S. and Dubé, J.F. (2008), "Global RC structural damage index based on the assessment of local material damage", *J. Adv. Concrete Technol.*, **6**(3), 459-468.

Belmouden, Y. and Lestuzzi, P. (2007), "Analytical model for predicting nonlinear reversed cyclic behaviour of reinforced concrete structural walls", *Eng. Struct.*, **29**(7), 1263-1276.

Buyukozturk, O. and Shareef, S.S. (1985), "Constitutive modeling of concrete in finite element analysis", *J. Comput. Struct.*, **21**(3), 581-610.

Cao, V.V. and Ronagh, H.R. (2013), "A model for damage analysis of concrete", *Adv. Concrete Constr.*, **1**(2), 187-200.

CEB-FIP (1993), "CEB-FIP Model Code 1990" Design Code, London, Telford.

CEB (1988), "Confined concrete", CEB-FIP Model code 1990, Supplementary Documents for the first predraft, Bulletin d'information, no. 189, July, Paris.

Chen, J.Y., Zhang, Z.X., Dong, H.W. and Zhu, J. (2011), "Experimental study on dynamic damage evolution of concrete under multi-axial stresses", *Eng. Failure Anal.*, **18**(7), 1784-1790.

Chore, H.S. and Shelke, N.L. (2013), "Prediction of compressive strength of concrete using multiple regression model", *Struct. Eng. Mech.*, **45**(6), 837-851.

Garcia Gonzalez, J.J. (1990), "Contribution á l'étude des poteaux en béton armé soumis á un cisaillement dévié alterné", Ph.D. Dissertation, University of Nantes/Ecole Central de Nantes, Nantes.

Karsan, I.D. and Jirsa, J.O. (1969), "Behavior of concrete under compressive loading", *J. Struct. Div.*, ASCE, **95**(ST12), 2543-2563.

LS-DYNA User Manual (2007), Version 971, Livermore Software Tech. Corp., Livermore, California, USA.

Mander, J.B., Priestley, M.J.N. and Park, R. (1984), "Theoretical stress-strain model for confined concrete", *ASCE J.*, **114**(8), 1804-1826.

Markovic, D. and Ibrahimbegovic, A. (2005), "Complementary energy based FE modeling of coupled elasto-plastic and damage behavior for continuum microstructure computations", *Comput. Meth. Appl. Mech. Eng.*, **195**(37), 5077-5093.

Markovich, N., Kochavi, E. and Ben-Dor, G. (2011), "An improved calibration of the concrete damage model", *Finite Elem. Anal. Des.*, **47**(11), 1280-1290.

Meyer, I.F. (1988), "Ein werkstoffgerechter schädigungs modell und stab abschnitts element für stahlbeton unter zyklischer nichtlinearer beanspruchung", *SFB 151, Mitteilung* No. 88-4, Bochum.

Otes, A. (1985), "Zur werkstoffgerechten Berechnung der Erdbebenbeanspruchng in Stahlbetontragwerken", *Mitteilungen aus dem Institut für Massivbau der TH Darmstadt*, Heft 25, Bochum.

Park, R., Kent, D.C. and Sampson, R.A. (1972), "Reinforced concrete members with cyclic loading", *J. Struct. Div.*, ASCE, **98**(ST7), 1341-1359.

Park, R., Priestley, M.J.N. and Gill, W.D. (1982), "Ductility of square-confined concrete columns", *J. Struct. Div.*, ASCE, **108**(ST4), 929-950.

Poinard, C., Malecot, Y. and Daudeville, L. (2010), "Damage of concrete in a very high stress state: experimental investigation", *Mater. Struct.*, **43**(1), 15-29.

Priestley, M.J.N. and Park, R. (1987), "Strength and durability of concrete bridge columns under seismic loading", *ACI Struct. J.*, **84**(1), 61-76.

Sadeghi, K. (1995), "Simulation numérique du comportement de poteaux en béton arme sous cisaillement dévié alterne", Ph.D. Dissertation, University of Nantes/Ecole Central de Nantes, Nantes.

Sadeghi, K. (2002), "Numerical simulation and experimental test of compression confined and unconfined concrete", Technical Report Submitted to Water Resources Management Organization, Ministry of Energy, Concrete Laboratory of Power and Water University of Technology, Tehran.

Sadeghi, K. (2015), "Nonlinear numerical simulation of RC columns subjected to cyclic oriented lateral force and axial loading", *Struct. Eng. Mech.*, **53**(4), 745-765.

Sadeghi, K., Nouban F. (2016), "Damage and fatigue quantification of RC structures", *Struct. Eng. Mech.*, **58**(6), 1021-1044.

Sheikh, S.A. (1982), "A comparative study of confinement models", *ACI J.*, ***79***(4), 296-305.

Sieffert, J.G., Lamirault, J. and Garcia, J.J. (1990), "Behavior of R/C Columns under Static Compression and Lateral Cyclic Displacement Applied out of Symmetrical Planes*", Proceedings of the First European Conference on Structural Dynamics (EUROPEAN 90)*, Vol. 1, Bochum, June.

Soh, C.K. and Bhalla, S. (2005), "Calibration of piezo-impedance transducers for strength prediction and damage assessment of concrete", *Smart Mater. Struct.*, **14**(4), 671-684.

Yu, T., Teng, J.G., Wong, Y.L. and Dong, S.L. (2010), "Finite element modeling of confined concrete-II: Plastic-damage model", *Eng. Struct.*, **32**(3), 680-691.

CC